Linking stimuli and behavior with fast near-whole brain recordings in adult Drosophila

Sophie Aimon[1], Takeo Katsuki[1], Logan Grosenick[2], Michael Broxton[2], Karl Deisseroth[3,4], Terrence J. Sejnowski[5,6], Ralph J. Greenspan[1,6,7]

[1] Kavli Institute for Brain and Mind, UCSD, La Jolla, CA 92093-0126, USA

[2] Departments of Computer Science and Bioengineering, Stanford University, Stanford, CA 94305, USA

[3] Departments of Bioengineering and Psychiatry, Stanford University

[4] Howard Hughes Medical Institute, Stanford University, Stanford, California, United States of America

[5] Howard Hughes Medical Institute, Computational Neurobiology Laboratory, Salk Institute for Biological Studies, La Jolla, CA 92037

[6] Division of Biological Sciences, University of California San Diego, La Jolla, CA 92093

[7] Department of Cognitive Science, University of California, San Diego, La Jolla, California, USA.

Abstract

We describe a method to record near-whole brain activity in behaving adult flies. Pan-neuronal calcium and voltage sensors were imaged at high speed with light field microscopy. Functional maps were then extracted by principal component analysis and independent component analysis. Their characteristic shapes match the anatomy of sub-neuropil regions and in some cases a specific neuron type. Responses to light and odor produced activity patterns consistent with previous techniques. Furthermore, the method detected activity linked to behavior as well as a previously uncharacterized pattern of spontaneous activity in the central complex.

Introduction

Measuring activity at the scale of the brain is essential for understanding how different brain regions interact to process and control sensory inputs, internal states and behavior. However techniques for imaging a whole brain so far have been orders of magnitude slower than the fastest neuronal electrical activity–recent reports of whole brain fluorescence imaging in Zebrafish and Drosophila larvae immobilized in a gel had a frame rate of 12 Hz (Tomer et al., 2015) and 5 Hz(Lemon et al., 2015) respectively. A newly developed technique, light field microscopy (Broxton et al., 2013; Grosenick, Anderson, & Smith, 2009; Levoy, Ng, Adams, Footer, & Horowitz, 2006; Prevedel et al., 2014), makes it possible to image large volumes at the frame rate of the fastest sCMOS cameras.

Here, we leverage this technique to record large-scale activity in the brain of behaving adult fruit flies. We show that the near-whole brain can be imaged with a 20x objective at a frame rate up to 200 Hz. We record the fluorescence of a pan-neuronally expressed calcium (GCaMP6 (Chen et al., 2013)) or voltage (Arclight (Jin et al., 2012)) probe. We apply computational methods (principal component analysis: PCA, and independent component analysis: ICA) to extract components representing spatially distinct sources of activity (Beckmann & Smith, 2004; Grosenick et al., 2009; Mukamel, Nimmerjahn, & Schnitzer, 2009). We show that these sources correspond to sub-neuropil areas or processes from small populations of neurons well characterized anatomically. Responses to flashes of light or odor puffs are consistent with literature reports of experiments done on restricted regions. Additionally, the method permits the discovery of new local and global patterns of activity.

Results

We prepared a fly so as to fix its head and expose its brain while maintaining the eyes, antennae and legs intact and clean (Figure 1-figure supplement 1). A ball was placed under the fly's tarsi so that it could typically rest, walk, or groom. We imaged the fly brain fluorescence using light field microscopy: as shown in Figure 1A, an upright epifluorescence microscope (equipped with a 20x NA=1.0 objective) was modified by adding a microlens array at the image plane of the objective, and placing the camera sensor at the image plane of the microlens array through relay lenses (Levoy et al., 2006). We recorded light field images continuously with a high speed sCMOS camera at 100 Hz for GCaMP6f, or at 200 Hz using half the camera frame for Arclight. We then reconstructed the volumes—typically 600 x 300 x 200 μm^3 to encompass the whole brain (Fig. 1B)—using the 3D deconvolution method for light field microscopy described in (ref. (Broxton et al., 2013)). Note that contrary to microscopy techniques based

on scanning (e.g. two-photon, confocal or light sheet microscopy), all of the brain is illuminated all the time, and all the photons going through the objective are used to reconstruct the image, thus maximizing the information flux from the brain activity to the signal on the camera. With 2 µm fluorescent beads embedded in a gel, we measured the point spread function and found that it widens with distance from the focal plane, varying from 3.5 to 12 µm laterally and from 6 to 35 µm axially (Figure 1-figure supplement 1). As shown below, this resolution was sufficient to extract activity from sub-neuropil compartments.

We applied statistical techniques: PCA and ICA, to extract maps and time series of spatially distinct sources of activity. We aligned the brain with an anatomical template(Ito et al., 2014) using landmarks registration to automatically sort the components by brain region. We then inspected the results in an interactive ipython-notebook to separate components likely due to brain activity from components likely due to movement or noise (see extracts from the notebook in Figure 2-figure supplement 4,5 and 6). Fig. 2 A shows a z-stack containing all the putative activity related maps (z-score>2.5) from a pan-neuronal GCaMP6f recording, while Fig. 2B shows the time series associated with each map (sorted by brain region). Different colors correspond to different components.

Even though PCA and ICA are mathematical algorithms that make minimal assumption about the brain, the majority of the functional maps matched well anatomical structures. In Fig. 3, the left column presents a selection of maps from Fig. 2, Fig. 2-figure supplement 1, or Fig. 2-figure supplement 2, whereas the right column presents central complex structures from (ref (Lin et al., 2013)) or neuronal processes from (ref. (Chiang et al., 2011)) assembled using Virtual Fly Brain (Milyaev et al., 2012). Several sub-neuropil regions are recognizable from the shape of the maps (e.g protocerebral bridge glomeruli, ellipsoid body rings and fan-shaped body layers). Note that the functional maps in the fan-shaped body and the lateral horn, are the same scale as functional maps obtained with higher resolution microscopy techniques ((Weir & Dickinson, 2015) and (Strutz et al., 2014) respectively), suggesting that the light field microscope's low resolution doesn't limit the detection of relevant functional regions. In some cases, a neuron type can be identified from the combination of sub-neuropil regions present in the map. For example, z-scored maps containing signal in one antennal lobe glomerulus, in the calix, and in the lateral horn, likely arise from the activity of one type of antennal lobe projection neurons. Likewise, z-scored maps with signals spanning both the horizontal and the vertical mushroom body lobes likely arise from activity in alpha-beta or alpha'-beta' Kenyon cells, while maps with signal in the horizontal lobe only likely arise from gamma Kenyon cells. Fig. 3 bottom and Fig. 2-figure supplement 2, show an

example of components obtained when using a more restrictive driver for dopamine neurons: TH-Gal4 (see also Fig. 4-figure supplement 1). The maps in Fig. 3 matched well with the anatomy of processes from dopaminergic PPL1 neurons innervating mushroom body alpha lobe compartments, each component thus corresponding to only one or two cells per hemisphere (Aso et al., 2014).

The component's time series are consistent with literature reports of the activity from the brain structures identified in the maps, and give insights into the activity related to both to stimuli and behavior in a same experiment. Components in the optic lobe strongly responded to onset and/or offset of light (Behnia, Clark, Carter, Clandinin, & Desplan, 2014) (Fig. 2 and Figure 2-figure supplement 5), while components in the antennal lobe and the lateral horn strongly responded to the odor puffs (Wilson, 2013). Note that components likely representing the activity of antennal projection neurons are spontaneously active in the absence of odor, but their activity strongly increases with the odor (Fig. 2-figure supplement 1 and Fig. 2-figure supplement 4)(Kazama & Wilson, 2009). In addition, regions in the lateral protocerebrum, the superior slope, the antennal mechanosensory and motor center, the saddle, and the protocerebral bridge were strongly active when the fly walked (Figure 2-figure supplement 6). This is consistent with the anatomy as the projection from the descending neurons are most dense in the posterior slope, ventrolateral protocerebrum, and the antennal mechanosensory and motor center(Hsu & Bhandawat, 2016). Note that the PCA/ICA algorithm helps to separate signals from artefacts such as movement or scattering from other part of the brain; however the interpretation of the time series should be made with care as the algorithm can also add some artefacts, or extract only a subpart of the neuron's activity (see Fig. 2-figure supplement 4, 5 and 6 as well as supplementary note for details about these limitations).

As shown in Fig. 4, voltage recordings with Arclight also gave rise to maps portraying specific neuropils. Even though these data were recorded in a single trial, the time series signal to noise ratio is high enough to detect clear graded potentials–e.g. components in the optic lobe in response to onset and offset of flashes of light, and spikes–e.g. odor response for components in the antennal lobe, calix and lateral horn, consistent with the literature(Wilson, 2013),(Behnia et al., 2014). The spikes are particularly visible in a more restricted driver for dopamine and serotonin neurons (TH-Gal4 and DDC-Gal4) as shown in Fig. 4-figure supplement 1. Note that the ability to record membrane voltage signals in the actual neuronal processes performing the computation is an advantage over patch clamp experiments, which can only be performed on the cell body at the periphery of the brain in Drosophila, and may thus be poorly representative of the activity in the neuronal processes (Gouwens & Wilson, 2009).

Previously unreported patterns of activity are also detected. Note for example the surprising spontaneous flip flop activity for components in a nodulus and contralateral protocerebral bridge (Fig. 4, second to last region and Figure 4-figure supplement 2 second and third components). As the time series resulting from the PCA/ICA algorithm match well with the time series from averaging in the region of interest (see ipython notebook), this pattern is dominant in the noduli and protocerebral bridge area. Although the fly wasn't moving in these experiments, the maps are similar to the pattern of expression of genetic drivers known to be involved in the fly's handedness (Buchanan, Kain, & de Bivort, 2015), while the time series resembles the flip flop pattern measured in the moth with intracellular recordings of neurons in the lateral accessory lobe(Namiki, Iwabuchi, Pansopha Kono, & Kanzaki, 2014) which is directly connected with the protocerebral bridge(Lin et al., 2013). Other unusual patterns of activity include slow continuous oscillations in the fan-shaped body, as well as slow oscillations after the second presentation of the odor in the antennal lobe, calix of the mushroom body, and superior neuropils. More work is needed to establish the conditions and consistency of these patterns of activity.

Applying PCA and ICA to large-scale recordings of adult fly brain activity allows the identification of sub-neuropil regions and in some cases neuronal types active in response flashes of light or odors, and correlated to walking. Although the method presented here has some limitations (see Supplementary Note), it can be used as a functional screen to identify brain regions and neurons involved in processing any stimulus or behavior that the fly can perform under the microscope–which greatly increases the possibilities compared to immobilized Zebrafish and Drosophila larvae. Furthermore, contrary to screens using activation or silencing of specific neurons, the component's time series give insight into the dynamics of the network, including ongoing spontaneous activity. This will help to understand how the brain implements various functions, in particular those involving many circuit loops, such as integrating stimuli with various types of memory to guide behavior (Aso et al., 2014) and situating the animal in space (Lin et al., 2013; Seelig & Jayaraman, 2015).

Methods

Fly rearing and preparation for imaging

The fly genotype was as described in Supplementary Table 1, and fly stocks were obtained from the Drosophila Bloomington Stock Center, Bloomington, IN. Flies were reared at 25 ^{o}C with a 24 h light/dark cycle on brown food (containing cornmeal, molasses, yeast, soy flour, agar, proprionate and nipogen) as it had a lower auto-fluorescence than yellow food (such as the one from the Bloomington Stock Center that contains yellow cornmeal, malt extract, corn syrup, yeast, soy flour, agar and proprionic acid).

Fly holders were 3D printed in black ABS (ordered from ZoomRP, with Supplementary data chamberb.stl). A piece of tape (Scotch 3M 0.75" Width) was shaped as a 1 mm high step using a 1 mm thick glass slide, and an aperture as in Supplementary Figure 1 (1mm wide for the body and 0.6 mm wide for the head) was made by hand using a sharpened scalpel or a thin lancet (36 gauge, TiniBoy). The tape was then stuck onto the chamber, aligning the opening of the tape to the center of the holder. To block the excitation light from hitting the fly's eyes, black nail polish (Black Onyx nail laquer, OPI products) was added onto the tape. Nail polish was also added at the contact between the tape and the holder to avoid leaks.

Flies were transferred to an empty glass vial and left on ice for approximately one minute. The holder was put in contact with wet tissues on ice under a stereomicroscope. A fly from the cold vial was pushed into the holder's opening so as to have the posterior part of the head well centered and in contact with the tape. UV-curing glue (Fotoplast gel, Dreve), was added at the junction between the tape and the head between the eyes and cured for five seconds using a 365 nm Thorlabs LED at 20% of power for 5s. A piece of thin copper wire (Wire-Magnet, 40 Gauge, AmplifiedParts) was placed above the legs to push them away from the proboscis (see Fig. 1-figure supplement 1). UV glue was then added at the rim of the eye and all around the proboscis, without touching the antenna or the legs, and cured for 5s. Uncured glue was carefully removed with tissues. The holder was then removed from the ice and cleaned again to remove humidity and any trace of remaining glue, and UV light was shone onto the head one last time to make sure that all the glue was cured. The wire was then removed, and a small piece of tissue paper or a small styrofoam ball was given to the fly to walk on to monitor its health during the following steps.

The holder was turned over and the fly's thorax was pushed down to clear the way to the back of the brain. Small pieces of tape were added onto any remaining holes around the fly's body, and UV glue was

added on top of them and cured around the thorax to fix it in place. Some glue was then pushed towards the neck with a very thin lancet needle (extracted from 36 Gauge tinyBoy lancets) and cured. Saline (108 mM NaCl, 5 mM KCl, 3 mM CaCl2,4 mM MgCl2, 4 mM NaHCO3, 1 mM NaH2PO4, 5 mM trehalose, 10mM sucrose, 5 mM HEPES adjusted to pH 3.5 +/- 0.5 with NaOH, prepared weekly) was added and left for few minutes to make sure that there were no leaks.

Fresh saline was added and dissection was started with forceps (#5SF, Dumont) that were priorly sharpened as finely as possible by hand. The cuticle in the middle of the back of the head was first removed, while being careful to cut pieces before pulling them out. This exposed the hole in the middle of the brain where muscle 16 resides. The pulsatile piece was pulled out. Fresh saline was added and the remainder of the cuticle was removed piece by piece. Glue was also gently scrubbed away if necessary. The brain was washed with saline several times to remove fat bodies. The air sacs were then removed very carefully to try not to displace the brain. After a new wash with saline, the fly was ready for imaging.

Imaging set up

The microscope was modified from an upright Olympus BX51W with a 20x NA 1.0 XLUMPlanFL objective (Olympus). A microlens array with pitch=125µm and f/10 to match the objective(Broxton et al., 2013) (RPC Photonics), was positioned at the image plane using a custom made holder (with some parts from Bioimaging Solutions, Inc). Two relay lenses (50mm f/1.4 NIKKOR-S Auto, Nikon) projected the image onto the sensor of a scientific CMOS camera (Hamamatsu ORCA-Flash 4.0). A 490nm LED (pE100 CoolLED) at approximately 10% of its full power was used for excitation. We used a 482/25 bandpass filter, a 495 nm dichroic beam splitter, and a 520/35 bandpass emission filter (BrightLine, Semrock) for the fluorescence. Note that the full set up was approximately 37000 dollars (52000 dollars with the 64Gb of Ram acquisition computer and the 256Gb of RAM analysis computers), which is an order of magnitude less than other cutting edge microscopy techniques such as two-photon microscopes.

The resolution as a function of depth (see Supplementary Figure 1) was determined by imaging 2 µm fluorescent beads dispersed in an agarose gel. After reconstruction, the center of beads at different distances from the focal plane was recorded using ImageJ, and a Matlab program measured the half height and half width of point spread function (see https://github.com/sophie63/FlyLFM for the code).

The fly holder was positioned on a U shaped stage above a floating ball so that the fly could walk (see Figure 1 and Supplementary Videos 2 and 3). The ball was either polyurethane foam (10 mm in

diameter), styrofoam, or hollow HDPE (¼ inch). A cup matching the ball diameter and with a 1.2 mm hole was prepared using self-curing rubber (Sugru). A bottle of compressed air provided a steady flow in a pipeline consisting of a tube and a pipette tip connected to the cup hole. A micromanipulator (Narishige) positioned the ball under the fly's legs. The fly and the ball were illuminated by a row of IR LEDs (940nm, RaspberryPiCafe®) in the front and back of the fly, and were observed at 100 Hz using a small camera (FFMV-03M2M, Point Grey).

For the odor stimulus, air was delivered by a pump (ActiveAQUA AAPA7.8L) through an electrically controlled valve (12 Vdc Normally Closed Solenoid Valve, American Science & Surplus), bubbled in 50% ethanol or 50% apple cider vinegar in a vial, and blown towards the fly through an inverted 1 mL pipette tip. The valve circuit was controlled by a relay (RELAY TELECOM DPDT 2A 4.5V, Digi-Key), connected to a labjack U3-HV through a LJTick-RelayDriver (LabJack). The excitation light and a 365nm or 470nm LED (Thorlabs) for visual stimulation, were also triggered by the LabJack, which was controlled using Matlab programs (see https://github.com/sophie63/FlyLFM for the code). In a typical experiment, the cameras for monitoring the behavior and the fluorescence were started first, and then the Matlab program was launched. The fluorescence images were recorded with HCImage (Hamamatsu) and streamed to RAM on a 64Gb of RAM computer, which allowed to record approximately 1 min of experiment continuously.

Analysis

The movies of the behavior were analyzed manually (pressing different keyboard keys when different behavior were recognized) using the Matlab GUI Video_Annotate in https://github.com/sophie63/FlyLFM. For Figure 2-figure supplement 4, 5 and 6, the fly's walk was measured tracking the movements of the ball using ImageJ's optic flow plugin (Gaussian Window MSE).

The light field images were reconstructed using a program in python as described in ref. (Broxton et al., 2013). Briefly, a point spread function library corresponding to the specific set up was first generated. Then the images were reconstructed using 3D deconvolution on a cluster of GPUs (generously provided by the Qualcomm Institute at UCSD). A dataset of 10000 time steps required approximately 8 hours to reconstruct on a cluster of 15 GPUs.

The images were assembled in a Nifti file using a python routine, and the first 5s were discarded as the strong activity in response to the excitation light made it difficult to correct for movement and photobleaching. The 3D image registration function 3dvolreg(Cox & Jesmanowicz, 1999) from AFNI was

then used to correct for movements in 3D. The background fluorescence, as well as the decrease in intensity from photobleaching, were removed by subtracting a signal smoothed using a box average over 10s. The time series were then multiplied by -1 for Arclight data. Although components could be extracted with unfiltered data, the number of components detected and the clarity of the maps were improved after first denoising the data. A Kalman filter (from https://www.mathworks.com/matlabcentral/fileexchange/26334-kalman-filter-for-noisy-movies) with a gain of 0.5 was better than a median filter over 3 points, and was used for the figures in this paper. The reconstructed data as well as the data after preprocessing will be soon available on the CRCNS website (https://crcns.org/NWB/Data_sets).

The average of the time series was aligned to an anatomical template (available here: https://github.com/VirtualFlyBrain/DrosAdultBRAINdomains) in which the brain is segmented in regions according to the nomenclature described in (Ito et al., 2014). The registration was performed using landmarks with ImageJ as described in http://imagej.net/Name_Landmarks_and_Register.

Dimensionality was then reduced by separating the volumes in slices of thickness corresponding to the point spread function half height, and averaging in z for each slice. The 4D data sets were typically (x,y,z,t)=200x100x10x10000 at this stage.

PCA and ICA were applied with a Matlab code using a fast SVD algorithm and Fastica (Hyvärinen, 1999) (see ICAalamelodic.m file from https://github.com/sophie63/FlyLFM), or using melodic (Beckmann & Smith, 2004) from the FSL package (for Fig. 4-supplementary figure 1). The principal component spectrum was inspected to determine the number of components. The sign was adjusted to have the average of the positive side of the map larger than the negative side. The components were then sorted by brain region, and a pruning was done by hand using an interactive ipython notebook (the notebooks corresponding to the choices made for the figures in this paper can be found at https://github.com/sophie63/FlyLFM). Only the components for which the maps were localized and the time series showed distinct patterns of activity such as spikes were kept. The other components likely corresponded to movement artefacts or noise, and imposing more components for PCA and ICA typically increased the number of noise components without affecting the components corresponding to brain activity.

Image manipulations

Figure 1B bar was added with ImageJ and the 3D rendering was done in Icy(de Chaumont et al., 2012), in which transparency and contrast were adjusted globally on the volume. The component's maps were thresholded at $2.5 \times \sigma$ in python (see the ipython notebooks), and only the positive part of the map is displayed. The image contrast was then adjusted globally in ImageJ and the figures were assembled in Inkscape.

Code availability

The Matlab and Python code for preprocessing, PCA/ICA and sorting of the components is available at: https://github.com/sophie63/FlyLFM.

Acknowledgements

We thank Jürgen Schulze, Joseph Keefe and Calit2 for generously providing a GPU cluster. Charles F. Stevens contributed many helpful discussions and comments on the manuscript. Angelique Paulk provided valuable advices on the floating ball set-up. Stephen M. Smith helped with reproducing parts of melodic in Matlab, Ryan Shultzaberger helped with R and bash, and Nicolas Aimon helped with fitting time series in python. M. Nitabach and V. Pieribone gave us UAS-Arclight flies and the Nitabach laboratory provided technical support on imaging Arclight.

Aso, Y., Hattori, D., Yu, Y., Johnston, R. M., Iyer, N. A., Ngo, T.-T. T., … Rubin, G. M. (2014). The neuronal architecture of the mushroom body provides a logic for associative learning. *eLife*, *3*, 1–48. http://doi.org/10.7554/eLife.04577

Beckmann, C. F., & Smith, S. M. (2004). Probabilistic independent component analysis for functional magnetic resonance imaging. *IEEE Transactions on Medical Imaging*, *23*(2), 137–52. http://doi.org/10.1109/TMI.2003.822821

Behnia, R., Clark, D. A., Carter, A. G., Clandinin, T. R., & Desplan, C. (2014). Processing properties of ON and OFF pathways for Drosophila motion detection. *Nature*, *512*(7515), 427–30. http://doi.org/10.1038/nature13427

Broxton, M., Grosenick, L., Yang, S., Cohen, N., Andalman, A., Deisseroth, K., & Levoy, M. (2013). Wave optics theory and 3-D deconvolution for the light field microscope. *Optics Express*, *21*(21), 25418–39. http://doi.org/10.1364/OE.21.025418

Buchanan, S. M., Kain, J. S., & de Bivort, B. L. (2015). Neuronal control of locomotor handedness in Drosophila. *Proceedings of the National Academy of Sciences of the United States of America*, *112*(21), 6700–5. Retrieved from http://www.pnas.org/content/112/21/6700.abstract

Chen, T.-W., Wardill, T. J., Sun, Y., Pulver, S. R., Renninger, S. L., Baohan, A., … Kim, D. S. (2013). Ultrasensitive fluorescent proteins for imaging neuronal activity. *Nature*, *499*(7458), 295–300. http://doi.org/10.1038/nature12354

Chiang, A.-S., Lin, C.-Y., Chuang, C.-C., Chang, H.-M., Hsieh, C.-H., Yeh, C.-W., … Hwang, J.-K. (2011). Three-dimensional reconstruction of brain-wide wiring networks in Drosophila at single-cell resolution. *Current Biology : CB*, *21*(1), 1–11. http://doi.org/10.1016/j.cub.2010.11.056

Cox, R. W., & Jesmanowicz, a. (1999). Real-time 3D image registration for functional MRI. *Magnetic Resonance in Medicine*, *42*, 1014–1018. http://doi.org/10.1002/(sici)1522-2594(199912)42:6<1014::aid-mrm4>3.0.co;2-f

de Chaumont, F., Dallongeville, S., Chenouard, N., Hervé, N., Pop, S., Provoost, T., … Olivo-Marin, J.-C. (2012). Icy: an open bioimage informatics platform for extended reproducible research. *Nature Methods*, *9*(7), 690–6. http://doi.org/10.1038/nmeth.2075

Gouwens, N. W., & Wilson, R. I. (2009). Signal propagation in Drosophila central neurons. *The Journal of Neuroscience : The Official Journal of the Society for Neuroscience*, *29*(19), 6239–49. http://doi.org/10.1523/JNEUROSCI.0764-09.2009

Grosenick, L., Anderson, T., & Smith, S. J. (2009). Elastic Source Selection for in vivo imaging of neuronal ensembles. In *Proceedings IEEE International Symposium on Biomedical Imaging: From nano to macro* (pp. 6–9). http://doi.org/10.1109/ISBI.2009.5193292

Hsu, C. T., & Bhandawat, V. (2016). Organization of descending neurons in Drosophila melanogaster. *Scientific Reports*, *6*, 20259. http://doi.org/10.1038/srep20259

Hyvärinen, A. (1999). Fast and robust fixed-point algorithms for independent component analysis. *IEEE Transactions on Neural Networks / a Publication of the IEEE Neural Networks Council*, *10*(3), 626–34. http://doi.org/10.1109/72.761722

Ito, K., Shinomiya, K., Ito, M., Armstrong, J. D., Boyan, G., Hartenstein, V., … Vosshall, L. B. (2014). A systematic nomenclature for the insect brain. *Neuron*, *81*(4), 755–765. http://doi.org/10.1016/j.neuron.2013.12.017

Jin, L., Han, Z., Platisa, J., Wooltorton, J. R. A., Cohen, L. B., & Pieribone, V. A. (2012). Single Action Potentials and Subthreshold Electrical Events Imaged in Neurons with a Fluorescent Protein Voltage Probe. *Neuron*, *75*(5), 779–785. http://doi.org/10.1016/j.neuron.2012.06.040

Kazama, H., & Wilson, R. I. (2009). Origins of correlated activity in an olfactory circuit. *Nature Neuroscience*, *12*(9), 1136–1144. http://doi.org/10.1038/nn.2376

Lemon, W. C., Pulver, S. R., Hockendorf, B., McDole, K., Branson, K., Freeman, J., & Keller, P. J. (2015). Whole-central nervous system functional imaging in larval Drosophila. *Nat Commun*, *6*. Retrieved from http://dx.doi.org/10.1038/ncomms8924

Levoy, M., Ng, R., Adams, A., Footer, M., & Horowitz, M. (2006). Light field microscopy. *ACM Transactions on Graphics*, *25*(3), 924. http://doi.org/10.1145/1141911.1141976

Lin, C. Y., Chuang, C. C., Hua, T. E., Chen, C. C., Dickson, B. J., Greenspan, R. J., & Chiang, A. S. (2013). A Comprehensive Wiring Diagram of the Protocerebral Bridge for Visual Information Processing in the Drosophila Brain. *Cell Reports*, *3*(5), 1739–1753. http://doi.org/10.1016/j.celrep.2013.04.022

Milyaev, N., Osumi-sutherland, D., Reeve, S., Burton, N., Baldock, R. a., & Armstrong, J. D. (2012). The virtual fly brain browser and query interface. *Bioinformatics*, *28*(3), 411–415. http://doi.org/10.1093/bioinformatics/btr677

Mukamel, E. A., Nimmerjahn, A., & Schnitzer, M. J. (2009). Automated analysis of cellular signals from large-scale calcium imaging data. *Neuron*, *63*(6), 747–760. Retrieved from http://www.ncbi.nlm.nih.gov/pubmed/19778505

Namiki, S., Iwabuchi, S., Pansopha Kono, P., & Kanzaki, R. (2014). Information flow through neural circuits for pheromone orientation. *Nature Communications*, *5*, 5919. http://doi.org/10.1038/ncomms6919

Prevedel, R., Yoon, Y.-G., Hoffmann, M., Pak, N., Wetzstein, G., Kato, S., … Vaziri, A. (2014). Simultaneous whole-animal 3D imaging of neuronal activity using light-field microscopy. *Nature Methods*, *11*(7), 727–30. http://doi.org/10.1038/nmeth.2964

Seelig, J. D., & Jayaraman, V. (2015). Neural dynamics for landmark orientation and angular path integration. *Nature*, *521*(7551), 186–191. http://doi.org/10.1038/nature14446

Strutz, A., Soelter, J., Baschwitz, A., Farhan, A., Grabe, V., Rybak, J., … Sachse, S. (2014). Decoding odor quality and intensity in the Drosophila brain. *eLife*, *3*, e04147. http://doi.org/10.7554/eLife.04147

Tomer, R., Lovett-Barron, M., Kauvar, I., Andalman, A., Burns, V. M., Sankaran, S., … Deisseroth, K. (2015). SPED Light Sheet Microscopy: Fast Mapping of Biological System Structure and Function. *Cell*, *163*(7), 1796–1806.

Weir, P. T., & Dickinson, M. H. (2015). Functional divisions for visual processing in the central brain of flying Drosophila. *Proceedings of the National Academy of Sciences of the United States of America*, *112*(40), E5523–32. http://doi.org/10.1073/pnas.1514415112

Wilson, R. I. (2013). Early olfactory processing in Drosophila: mechanisms and principles. *Annual Review of Neuroscience*, *36*, 217–41. http://doi.org/10.1146/annurev-neuro-062111-150533

Figure 1: Imaging the fly brain using light field microscopy. A) Experimental set up. The fly is head fixed and its tarsi are touching a ball. The light from the brain goes through the objective, the microscope tube lens, a microlens array, and relay lenses, onto the sensor of a high-speed sCMOS camera. The behavior is recorded with another camera in front of the fly. B) Example of a light field deconvolution. Top: 2D light field image acquired in 5ms with a 20x NA 2.0 objective. Bottom: Anterior and posterior views (slightly tilted sideways) of the computationally reconstructed volume. 3D bar is 90x30x30 microns.

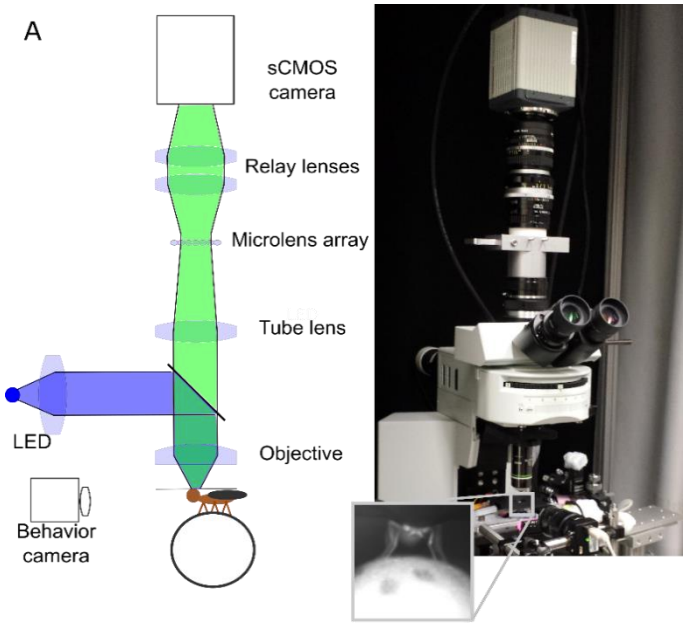

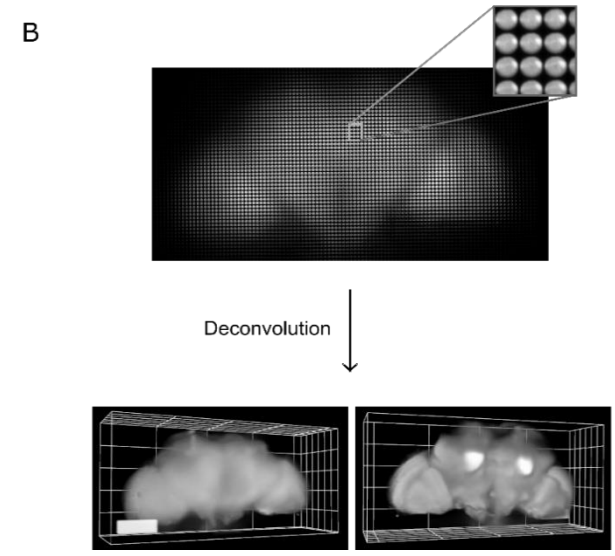

Figure 2: Z-scored maps and time series of the sources extracted using PCA and ICA for an experiment in which flashes of UV light were presented to a fly expressing GCaMP6f pan-neuronally. A) Z-stack maps.

Different colors correspond to different components. B) Time series (left) associated with the maps (right) sorted by brain regions and projected along the z axis. Flashes of UV light are indicated in purple, and the moments when the fly walks are in forest green (in gray is a time period during which the fly'sbehavior was unclear). Bar: 90μm.

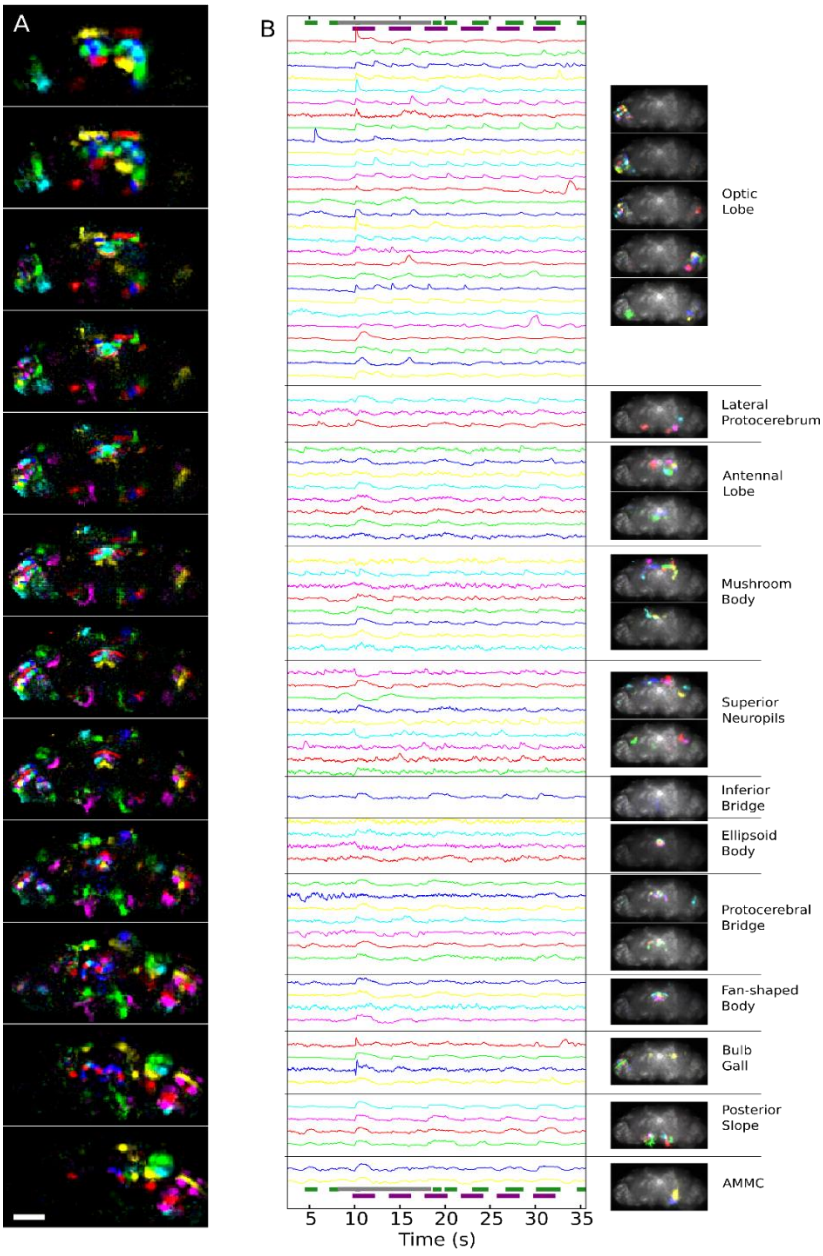

Figure 3: Comparison between functional and anatomical maps. Left: functional maps chosen from Fig. 2, Fig. 2-supplement figure 1, and Fig. 2-supplement figure 2 (UAS-GCaMP6F flies). Right: corresponding anatomical structures. Top three other images correspond to central complex structures–modified from Cell Reports, Vol. 3, Lin, C. Y. et al.," A Comprehensive Wiring Diagram of the Protocerebral Bridge for Visual Information Processing in the Drosophila Brain.," 1739-1753, Copyright 2013, with permission from Elsevier, and four bottom images were neurons chosen in the Virtual Fly Brain database.

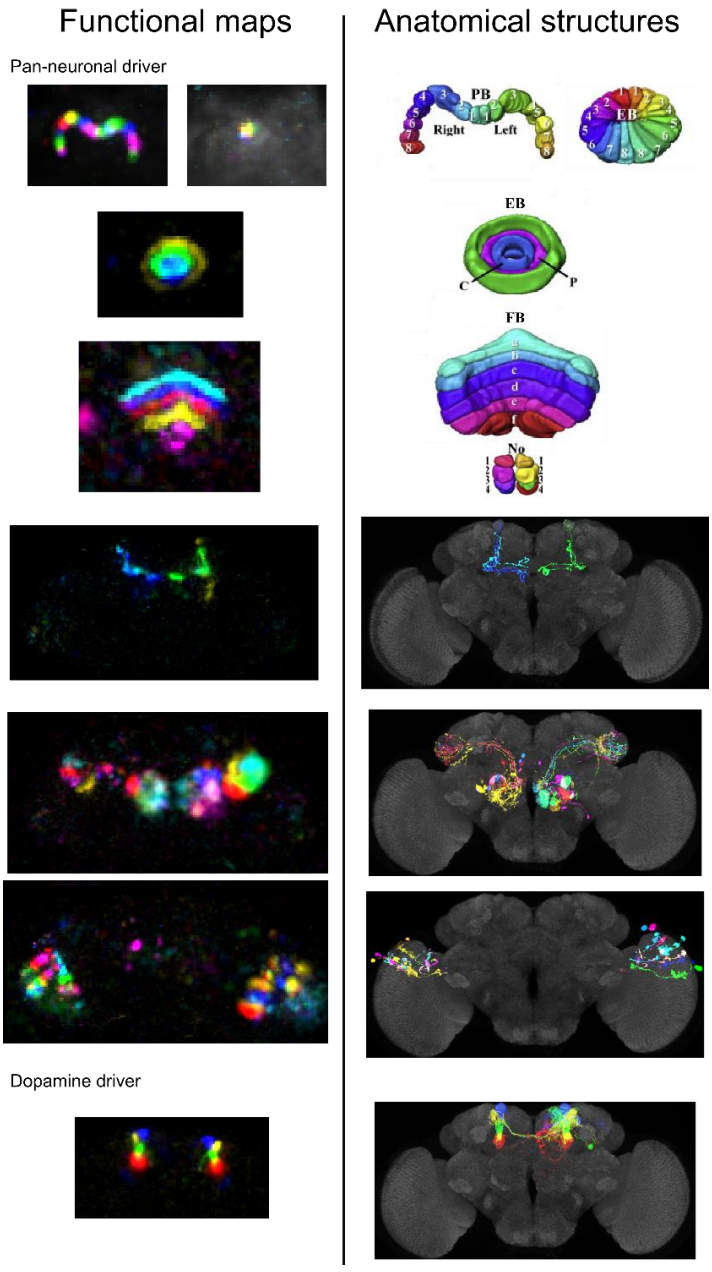

Figure 4: Components extracted from whole brain voltage activity. Arclight was expressed pan-neuronally (nSyb-GAL4). The fly was presented periodic flashes of UV light (violet bars) and puffs of apple cider vinegar (pink bars). Shown on the left are the component time series, while on the right are the corresponding maps (PB: protocerebral bridge, FB: fan-shaped body), sorted by brain region majorly present in the map.